A modular model of Jupiter's magnetospheric magnetic field based on Juno data

Jian-zhao Wang[1], Zhuo-xi Huo[1], and Lei Zhang[1]

[1]Qian Xuesen Laboratory of Space Technology

November 23, 2022

Abstract

Accurate modeling of Jupiter's magnetospheric magnetic field is important for not only scientific research but also mission planning. We develop a new empirical global model of Jupiter's magnetic field in the Juno era, including components from the planetary dynamo, Chapman-Ferraro currents, and cross-tail current sheet. The internal field is based on the JRM09 model. The shielding field is obtained by minimizing the component normal to Jupiter's magnetopause and varies due to the change of solar wind dynamic pressure. Combined with the curved magnetodisk, the high-resolution TS07 method is used for modeling Jupiter's magnetodisc and tail currents. The best-fitting results show an asymmetric magnetodisc current system in azimuthal direction with a tilted angle to Jupiter's magnetic equator. The sweep-back effects of Jupiter's magnetic fields are also reproduced by the radial current system. This new model is validated by comparing with Juno's magnetometer data in the range from 5 Rj to 60 Rj, where Rj=71492 km is the radius of Jupiter.

Posted on 23 Nov 2022 — The copyright holder is the author/funder. All rights reserved. No reuse without permission. — https://doi.org/10.1002/essoar.10506065.1 — This a preprint and has not been peer reviewed. Data may be preliminary.

A modular model of Jupiter's magnetospheric magnetic field based on Juno data

Jian-zhao Wang[1], Zhuo-xi Huo[1], Lei Zhang[1]

[1]Qian Xuesen Laboratory of Space Technology, China Academy of Space Technology, Beijing, China

Key Points:

- A Jupiter's global magnetic field model is built, including fields from the planetary dynamo, current sheet, and magnetopause current.
- The magnetopause and the current on it are dynamically modeled based on solar wind dynamic pressure.
- A tilted asymmetric current system on the magnetic equator is reproduced and the sweep-back effect is incorporated in the current sheet model.

Corresponding author: Jian-zhao Wang, `wangjianzhao@qxslab.cn`

Abstract

Accurate modeling of Jupiter's magnetospheric magnetic field is important for not only scientific research but also mission planning. We develop a new empirical global model of Jupiter's magnetic field in the Juno era, including components from the planetary dynamo, Chapman-Ferraro currents, and cross-tail current sheet. The internal field is based on the JRM09 model. The shielding field is obtained by minimizing the component normal to Jupiter's magnetopause and varies due to the change of solar wind dynamic pressure. Combined with the curved magnetodisk, the high-resolution TS07 method is used for modeling Jupiter's magnetodisc and tail currents. The best-fitting results show an asymmetric magnetodisc current system in azimuthal direction with a tilted angle to Jupiter's magnetic equator. The sweep-back effects of Jupiter's magnetic fields are also reproduced by the radial current system. This new model is validated by comparing with Juno's magnetometer data in the range from 5 R_j to 60 R_j, where $R_j = 71492$ km is the radius of Jupiter.

1 Introduction

The modeling of Jupiter's magnetic field helps understand the particle dynamics, magnetospheric dynamics, and coupling processes between the magnetosphere and ionosphere. Jupiter's magnetosphere is highly coupled with its moon. The neutrals from Io are outward and can be ionized as ions because of geologic activities (Russell et al., 2004). The ions are the main sources of the dense plasma torus near the equator in the inner region ($< 10R_j$, $R_j = 71492$ km is the radius of Jupiter) and the torus nearly corotates with the planet due to strong magnetosphere-ionosphere-atmosphere coupling.(Bagenal, 1994). In the middle region ($10-40R_j$), the plasma corotation with Jupiter's magnetosphere gradually breaks down. The thin current sheet locates near the equator and the magnetic field becomes highly stretched (Cowley et al., 2002). In the outer region ($> 40R_j$), the configuration of the magnetosphere is highly dependent on the solar wind. On the dayside, the distance of magnetopause varies from $45R_j$ to $100R_j$ depending on the solar wind dynamic pressure (Joy et al., 2002). On the nightside, the magnetotail current system connects the magnetodisk current to the magnetopause current. This current system stretches the field line and creates a long magnetotail, which extends to the orbit of Saturn (McComas et al., 2017). Furthermore, the accurate modeling of Jupiter's magnetic field is also important for engineering. Energetic particles are trapped by the magnetic field. The maximum energies of electrons and protons can be higher than 100 MeV and 1 GeV, relatively. These particles are harmful to electronics in spacecraft and radiation effects caused by them are the main constrains of Jupiter mission design (Fieseler et al., 2002; Wang, Zhang, et al., 2019; Wang, Ma, et al., 2019).

One important source of Jupiter's magnetic field is the dynamo field, which is associated with the metallic-hydrogen region of Jupiter's interior (Jones, 2014). The modeling attempts of the internal field started from the Jupiter flybys of Pioneer 10/11. The O4 model (Acuna & Ness, 1976) adopted the data of magnetometers onboard these two spacecraft and included the first three orders and degrees of the spherical harmonics. After including data from the Voyager 1 flyby, Connerney et al. (1982) developed the O6 model, which is reliable for the first three orders and matches the Ulysses observations very well (Dougherty et al., 1996). This model assumed the intrinsic field was immutable from the Pioneer era to the Voyager era and included the contribution of Jupiter's current sheet. Combining the in-situ data from Pioneer and Voyager and the observations of locations of Io flux tube footprints in Jupiter's ionosphere, Connerney et al. (1998) improved the previous models to a higher precision by including the fourth-order. Furthermore, Randall (1998) derived a new model that can reproduce the absorption micro signature of the moon Amalthea.

Before the Juno era, Pioneer 11 provided the best description of the internal field because of its retrograde orbit and high inclination. Modeling higher-order terms of Jupiter's internal field is difficult because of limited datasets. Although Galileo orbited Jupiter for about eight years, the limitation of its latitudinal coverage is unsuitable for improving these models. After JOI (Jupiter Orbit Insertion) in July 2016, Juno provided a global coverage observation of Jupiter' magnetic field with perijove of 1.05 R_j and longitudinal separation of 45° between perijoves (Bagenal et al., 2017). Based on Juno's observations of its first nine orbits, Connerney et al. (2018) established a new model named JRM09. The spherical harmonic coefficients of this model are well determined through degree and order 10. JRM09 provided the detailed view of Jupiter's complex dynamo and shows the hemispheric dichotomy of Jupiter's magnetic field (Moore et al., 2018). The non-dipolar part of the field is confined to the northern hemisphere and the field in the southern hemisphere is predominantly dipolar. This suggests the radial variations in density and electrical conductivity in Jupiter's interior.

Another important source of Jupiter's magnetic field is the field generated from the ring current near the equatorial plane and the tail current system (Alexeev & Belenkaya, 2005). Since the discovery of Jupiter's current sheet, many models have been created. Connerney et al. (1981) modeled the azimuthal current sheet by a finite thickness and became the basis of many other empirical models. This model assumed that the current density is uniform within the width of the disk and is inversely proportional to the distance from the magnetic axis. This model fits the observations of Pioneer 10 and Voyager 1/2 well within $\sim 30\ R_j$. In the Galileo era, another approach was developed by Khurana (1997) and described the fields in terms of Euler potentials. This model includes sweep-back effects of the magnetic field lines. In the Juno era, new current sheet models are developed. Pensionerov, Belenkaya, et al. (2019) fitted the best optimal parameters of magnetodisc using Juno's data. Furthermore, Pensionerov, Alexeev, et al. (2019) incorporated models of Connerney et al. (1981) and Khurana (1997) in a piecewise fashion to more accurately model the field within $\sim 95\ R_j$ and termed the model as the PCD model. Based on measurements of Juno's first 24 orbits, Connerney et al. (2020) established a new tilted current disk model supplementing by an outward radial current system.

Besides the model of Khurana (1997), all other models are based on an assumption that equatorial current is symmetric along the azimuthal direction and could not describe the sweep-back nature of Jupiter's magnetic field. However, the structure of the current disk is complex and time-dependent, including asymmetries of current density and thickness of the current sheet (Khurana & Schwarzl, 2005; Lorch et al., 2020). These complex asymmetries arise from both internal rotational stresses and external solar wind forcing on the system (Arridge et al., 2015). In recent years, techniques for modeling the Earth's magnetic field in its magnetosphere were developed rapidly and an overview is from Tsyganenko (2013). Tsyganenko and Sitnov (2007) presented an empirical modeling method (hereafter TS07) based on large sets of data. In this method, the magnetic field is expanded into a sum of orthogonal basis functions and is capable to reproduce arbitrary radial and azimuthal current distribution. This method abandons the idea of a predescribed equatorial current system and could reveal dynamical characteristics during storm time (Sitnov et al., 2008; Stephens et al., 2016). With an abundance of in-situ magnetometer data from Galileo and Juno, These techniques could advance the current sheet model of the Jovian system.

To filter data outside the magnetopause, shielding field from magnetopause currents (Chapman-Ferraro currents) should also be considered. Combining in-situ data and magnetohydrodynamic (MHD) simulation, Joy et al. (2002) presented probabilistic models of the Jovian magnetopause and bow shock. In the model, the size of the magnetopause is parameterized by solar wind dynamic pressure. Furthermore, statistics show a bimodal distribution of boundary positions of Jupiter's magnetopause (McComas et al., 2014; Col-

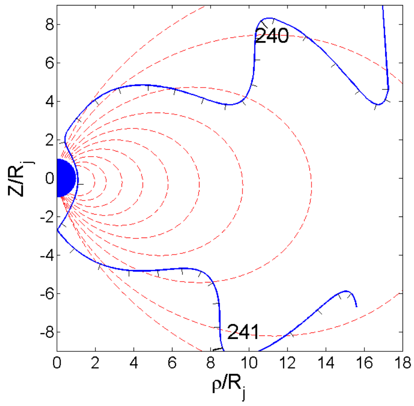

Figure 1. Juno trajectory plot for Perijove 1 in magnetic equatorial coordinates on 27 August (day 240) 2016. The tick marks are given every hour.

lier et al., 2020), i.e. the compressed and expanded magnetosphere. Tsyganenko (1995) developed a magnetopause current modeling method by minimizing the normal component of the total magnetic field on the magnetopause surface. To better understand the dynamic nature of Jupiter's magnetosphere, all these magnetic field sources should be included to improve the current models. In this study, we attempt to build a global model of Jupiter's magnetosphere including internal field, asymmetric equatorial current system, and magnetopause current.

2 Data

We utilize the fluxgate magnetometer data of Juno mission up to the 24th perijove (PJ) (Connerney et al., 2017). Juno was inserted into the polar orbit of Jupiter with a perijove of $\sim 1.05R_j$ and an apojove of $\sim 113R_j$. The Juno mission was designed to wrap the planet in a dense net of observations using perijove passes evenly spaced in longitude about the planet. The trajectories of Juno for PJ1 are shown in Fig. 1. The vertical axis is aligned with Jupiter's planetary dipole. Also illustrated in the plot are the magnetic field lines. The spacecraft appears to wiggle up and down because of Jupiter's rotation with a period of about 10 hours and the angular offset of the dipole from the spin axis. In such orbits, Jupiter is globally coveraged and magnetodisk currents are sampled when Juno penetrates into and passes through the current-carrying region near the magnetic equator.

The vector magnetic field is measured continuously and sampled at a rate of 64, 32, and 16 samples per second depending on the distance from Jupiter. In this study, we use the data that has been downsampled to 1 minute and provide a compact dataset. The data are archived and available at the PDS (Planetary Data System)[1]. We further average the data by 5-min interval for analysis and the time resolution is high enough for characterization of Jupiter's magnetosphere.

[1] https://pds-ppi.igpp.ucla.edu/search/view/?f=yes&id=pds://PPI/JNO-J-3-FGM-CAL-V1.0

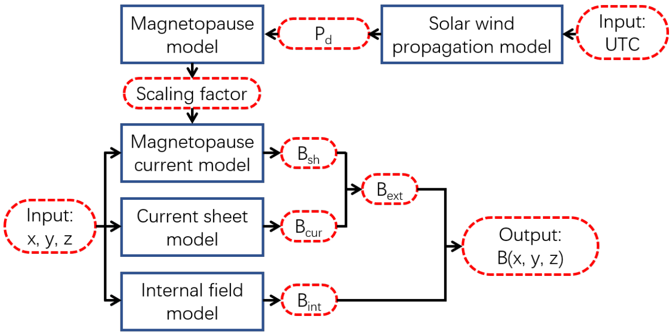

Figure 2. The structure of Jupiter's magnetic field modular model.

3 Model structure and results

3.1 Magnetospheric magnetic field

The total magnetic field $\boldsymbol{B}_{tot}$ in Jupiter's magnetosphere consists of contributions from internal part $\boldsymbol{B}_{int}$ and external part $\boldsymbol{B}_{ext}$. $\boldsymbol{B}_{int}$ is the planetary field and generated by the complex dynamo mechanism. $\boldsymbol{B}_{ext}$ is associated with currents flowing inside Jupiter's magnetosphere, including fields from cross-tails current $\boldsymbol{B}_{cur}$ and that from magnetopause currents (Chapman-Ferraro currents) $\boldsymbol{B}_{sh}$.

$$\begin{cases} \boldsymbol{B}_{tot} = \boldsymbol{B}_{int} + \boldsymbol{B}_{ext} \\ \boldsymbol{B}_{ext} = \boldsymbol{B}_{cur} + \boldsymbol{B}_{sh} \end{cases} \tag{1}$$

The model's structure is shown in Fig. 2. The inputs are Coordinated Universal Time (UTC) and the coordinate. The output is the corresponding vector magnetic field. The solar wind propagation model is used to calculate the solar wind dynamic pressure (P_d) in Jupiter's orbit at a given UTC. P_d determines the shape of the magnetopause and the corresponding scaling factors. After the magnetopause is determined, $\boldsymbol{B}_{sh}$ is obtained by shielding the internal field. Finally, we obtain the total magnetic field combining $\boldsymbol{B}_{ext}$ with the internal field.

Conventionally, different sources of fields are built on different coordinate systems. $\boldsymbol{B}_{int}$ is usually built on IAU standard Jupiter System III coordinates (Riddle & Warwick, 1976), in which the Z-axis is defined by the spin axis of Jupiter. $\boldsymbol{B}_{sh}$ is built on Jupiter-Sun-Orbit (JSO) coordinates (Bagenal & Wilson, 2016), in which the X-axis is aligned with the Jupiter-Sun vector and the Y-axis is antiparallel to the vector of Jupiter's motion. $\boldsymbol{B}_{cur}$ is built on Jupiter magnetic coordinates, in which the Z-axis is aligned with Jupiter's magnetic dipole and the Y-axis is aligned with the intersection of the magnetic and geographic equator. See the Appendix section in Bagenal et al. (2017) for details about these coordinate systems. In the following sections, we will discuss how to model and combine each part of the fields.

3.2 The internal magnetic field

The internal magnetic field can be represented as the gradient of a scalar potential: $\boldsymbol{B}_{int} = -\nabla\Phi_{int}$. So the standard solution to the Laplace's equation is used to describe the field (Connerney et al., 2017). The solution of scalar potential in the Jupiter System III coordinate is given by the sum of spherical harmonics:

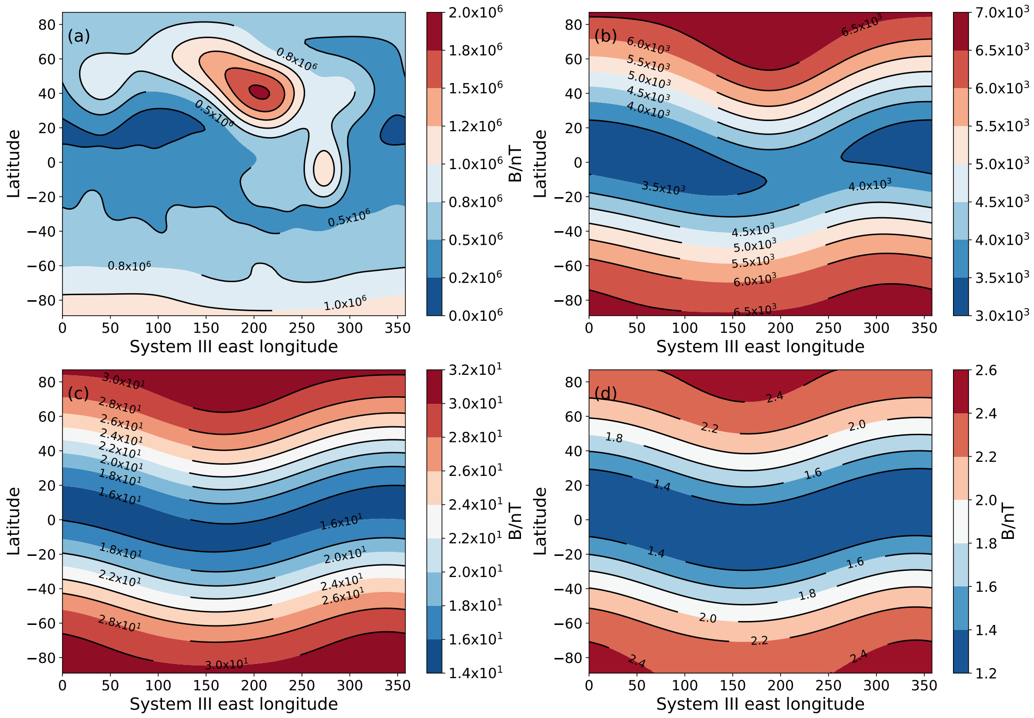

Figure 3. Contours of the internal magnetic field magnitude at (a) $1R_j$, (b) $5R_j$, (c) $30R_j$, and (d)$70R_j$ from Jupiter's center in rectangular latitude-longitude projection.

$$\Phi_{int}(r,\theta,\phi) = \sum_{n=1}^{\infty}(\frac{R_j}{r})^{n+1}\sum_{m=0}^{n}P_n^m(\cos\theta)[g_n^m\cos(m\phi)+h_n^m\sin(m\phi)] \tag{2}$$

where r is the distance from the planet's center, θ and ϕ are the corresponding colatitude and longitude, P_n^m is the associated Legendre polynomial function, g_n^m and h_n^m are the Schmidt coefficents of order n and degree m.

In this study, we choose the JRM09 model as the internal field model. The coefficients of this model are well determined through degree 10 and provide the most detailed view of a planetary dynamo other than the Earth. Furthermore, Stallard et al. (2018) gave evidence supporting an immutable intrinsic field between the Galileo era and the Juno era. Some results from the JRM09 model are shown in Fig. 3. In general, $\boldsymbol{B}_{int}$ decrease very fast with increasing r. Comparing with the higher-order field, the dipole field is dominant beyond 5 R_j because the dipole field is proportional to r^{-2} and the quadrupole field is proportional to r^{-4}, etc. So the higher-order field decreases much faster than the dipole field. As a result, the subplots (b), (c), and (d) are essentially symmetric in ϕ and θ directions.

3.3 Shielding magnetic field from the magnetopause

3.3.1 Modeling method

At Jupiter's magnetopause, the pressure balance between the external solar wind dynamic pressure and internal magnetic and plasma pressure is achieved. Joy et al. (2002)

used a quasi-paraboloid model to describe the shape of Jupiter's magnetopause in JSO coordinates:

$$z^2 = A(P_d) + B(P_d)x + C(P_d)x^2 + D(P_d)y + E(P_d)y^2 + F(P_d)xy \tag{3}$$

where the coefficients $(A-F)$ are functions of solar wind dynamic pressure P_d. Combining observations and MHD simulation, $A-C$ and $D-F$ are linear functions of $P_d^{(-1/4)}$ and P_d, relatively.

The magnetopause carries electric currents that shield the magnetosheath from the field inside the magnetosphere. So, the magnetopause shielding field $\boldsymbol{B}_{sh}$ corresponds to a zero normal component of the total field vector at the boundary. $\boldsymbol{B}_{sh}$ is curl free and can be represented as the gradient of a scalar function:

$$\boldsymbol{B}_{sh} = -\nabla U_{sh} \tag{4}$$

where U_{sh} is the scalar funtion and can be represented by a series expansion of basis funtion in cylindrical coordinate system (Tsyganenko, 1995):

$$U_{sh} = \sum_{i=1}^{N} a_i J_1(\frac{\rho}{b_i}) \exp(\frac{x}{b_i}) \sin\phi \tag{5}$$

where J_1 is Bessel function of the first kind and order 1. a_i and b_i are parameters and can be calculated by minimizing the normal component of the total magnetic field on the magnetopause using downhill simplex algorithm (Press et al., 1992):

$$\sigma_{sh} = \sqrt{\sum_{i=1}^{N}[(\boldsymbol{B}_{int}^{(i)} - \nabla U_{sh}^{(i)}) \cdot \boldsymbol{n}^{(i)}]/N} \tag{6}$$

where $\boldsymbol{B}_{int}^{(i)}$ is the magnetic field from internal source to be shielded at the i-th location. $\boldsymbol{n}^{(i)}$ is the unit vector normal to the magnetopause surface at the i-th location. One example of shielding effects of magnetopause currents is shown in Fig. 4. The fitting results correspond to the situation that $P_d = 0.045$ nPa. After adding the shielding field, the magnetic field is fully confined inside the magnetopause.

3.3.2 Scaling of the magnetopause

The magnetopause expands and contracts with changes to the solar wind dynamic pressure in a self-similar way. A spatial rescaling method is applied to adjust the self-similar behavior and the magnetopause coefficients do not need to change due to different solar wind dynamic pressure.

$$\begin{cases} [x', y', z'] = [S_x, S_y, S_z] \cdot [x, y, z] \\ \boldsymbol{B}'_{sh} = S_x S_y S_z \boldsymbol{B}_{sh} \end{cases} \tag{7}$$

where $\boldsymbol{B}'_{sh}$ is the adjusted magnetic field. (x', y', z') is the adjusted location of coordinate (x, y, z). $S_x/S_y/S_z$ is the scaling parameter in the $x/y/z$ direction and varies with solar wind dynamic pressure. Based on the data of Table 1 in Joy et al. (2002), a logarithmic linear regression is made between pressure and magnetopause size. The results are shown in Fig. 5. X_{pause}, Y_{pause}, and Z_{pause} are the boundary locations along the respective axes in given P_d from Joy et al. (2002). There is no surprise about the good

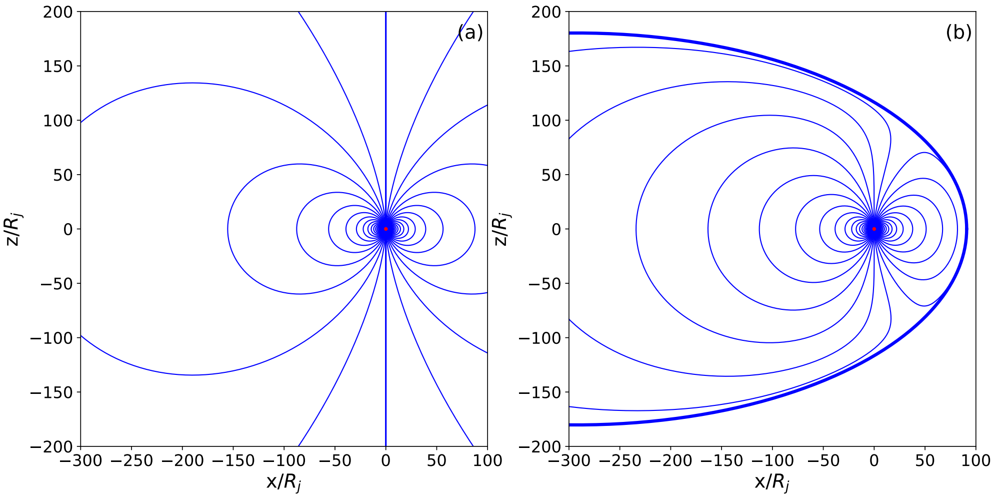

Figure 4. (a) Unshielded and (b) shielded magnetic field lines for dipole field.

results because A–F in Equ. 3 are also linear functions of $P_d^{(-1/4)}$ and P_d. Then the scaling parameters can be obtained as a function of solar wind dynamic pressure:

$$\log_{10}(S_i) = a_i \cdot \log_{10}(P_d) + b_i, (i = x, y, z) \tag{8}$$

where a_i and b_i are parameters in the i-axis. The values of a_i and b_i are also shown in Fig. 5. In the fitting, we assume the scaling parameters for $P_d = 0.045$ nPa are 1. An illustration of how the solar wind dynamic pressure control Jupiter's magnetospher is shown in Fig. 6. Under the premise that the magnetic field is confined in the magnetopause, the magnetosphere is expanded or compressed with the change of P_d. While P_d varies from 0.045 nPa to 0.36 nPa, the boundary of magnetopause is compressed from $91R_j$ to $55R_j$.

To develop a real-time model, the solar wind dynamic pressure at any given time should be simulated. So we adopt the solar wind propagation model developed by Tao et al. (2005). This model takes observations of solar wind in near-Earth space and uses a 1-D MHD model to propagate solar wind to 10 AU. This model can simulate dynamic pressure, density, velocity, and interplanetary magnetic field in Jupiter's orbit, and the results from the model were validated by Zieger and Hansen (2008). The P_d data from the model are now available on the AMDA archive.[2]

3.4 Magnetic field from the current sheet

The magnetic field line is greatly distended from the planet by the dawn-to-dusk current near the magnetic equator, which is responsible for the enormous size of Jupiter's magnetosphere. In the previous models, the current sheet is always assumed as a symmetric azimuthal (dawn-to-dusk direction) configuration while the current density decreases with the distance from the planet. However, from a detailed analysis by Lorch et al. (2020), the current density varies with local time and the radial current should also be considered. So we employ the TS07 method (Tsyganenko & Sitnov, 2007) to construct the complex morphologies of equatorial current system. This method does not impose

[2] http://amda.cdpp.eu/

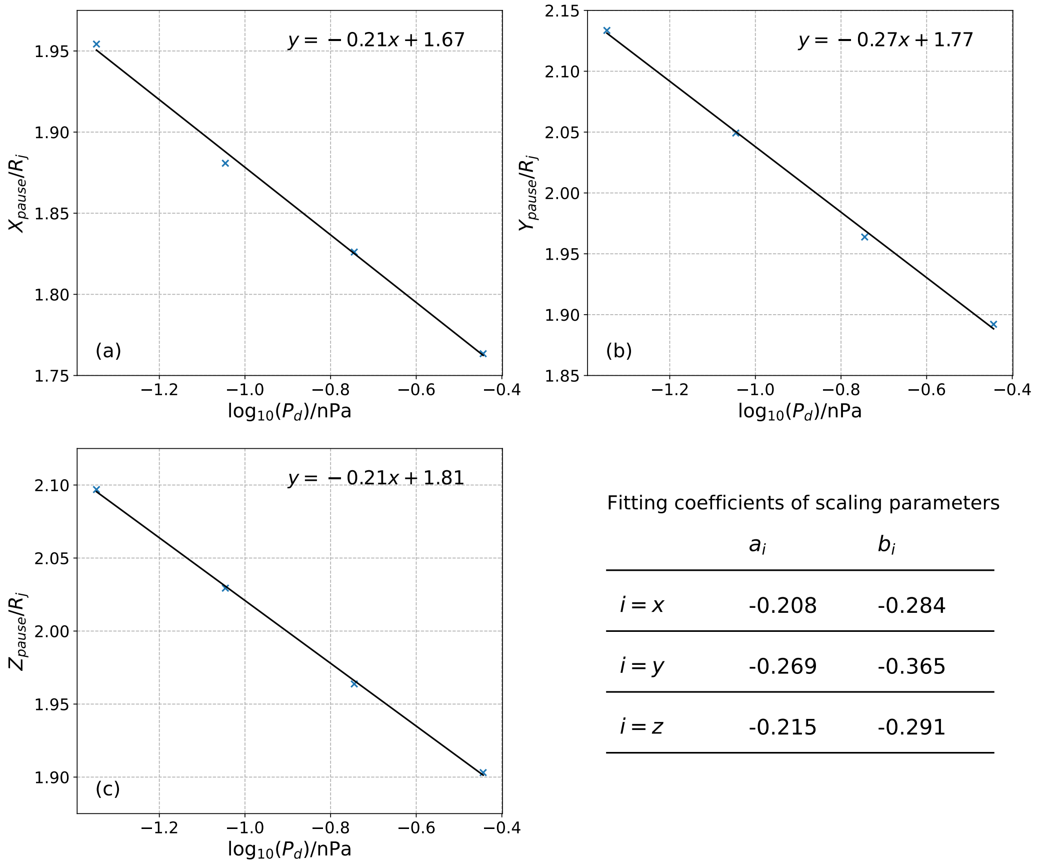

Figure 5. The linear regression between logarithmic solar wind pressure and magnetopause size in (a) X-axis, (b) Y-axis, and (c) Z-axis. Also shown are the fitting coefficients to scaling parameters of Equ. 8.

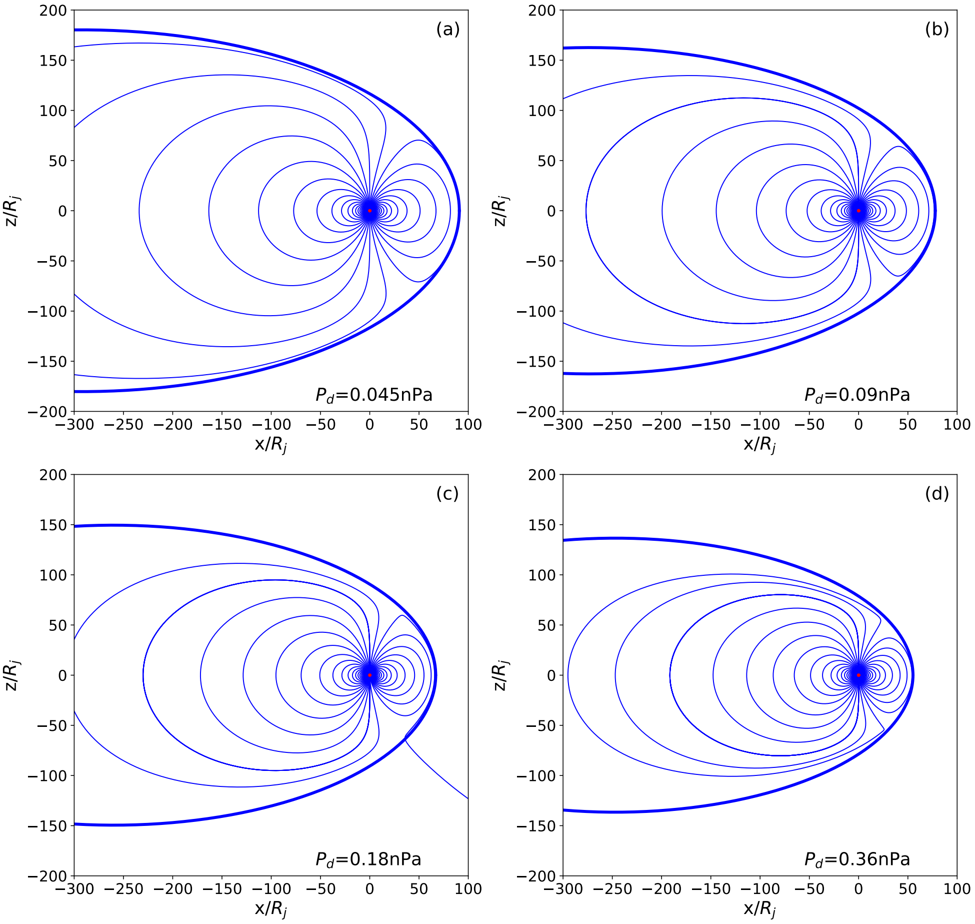

Figure 6. The change of the magnetospheric configurations due to different solar wind dynamic pressures. The thin and thick lines represent the magnetic field lines and the configuration of magnetopause, respectively.

a predefined azimuthal or radial current sheet. After fitting in-situ data, TS07 can describe any distribution of current in the equatorial sheet (tail and ring systems) with finite sheet thickness by a regular expansion into series of basis functions:

$$\boldsymbol{B}_{cur}(\rho,\phi,z) = \sum_{n=1}^{N} a_n^{(s)} \boldsymbol{B}_n^{(s)} + \sum_{m=1}^{M}\sum_{n=1}^{N} a_{mn}^{(o)} \boldsymbol{B}_{mn}^{(o)} + \sum_{m=1}^{M}\sum_{n=1}^{N} a_{mn}^{(e)} \boldsymbol{B}_{mn}^{(e)} \tag{9}$$

where $\boldsymbol{B}_{curr}$ is the field from equatorial current system represented by the TS07D model. $\boldsymbol{B}_{\alpha\beta}^{(\gamma)}$ is the basis function and $a_{\alpha\beta}^{(\gamma)}$ is the weight from the fitting procedure. M and N are parameters, which determine the number of expansion terms. The formula of $\boldsymbol{B}_{\alpha\beta}^{(\gamma)}$ can be found in Tsyganenko and Sitnov (2007). The solution is combined by azimuthally symmetric modes denoted by the index (s) and asymmetric modes denoted by the index (o) and (e), corresponding to odd and even components with respect to the plane $y = 0$, relatively. The spatial resolution of the equatorial current sheet is determined by (M, N) and can be increased to the desired value by increasing the values of M and N. However, a model with too many degrees of freedom will be subject to overfitting, whereas an underfit model will not fully capture the breadth of information contained in the data. In this study, we choose $(M, N) = (10, 10)$ by trial and error.

To fit the current distribution in Jupiter magnetic coordinate, the optimal values for coefficients $a_{\alpha\beta}^{(\gamma)}$ are searched out by using the downhill simplex algorithm and minimizing the error:

$$\sigma_{cur} = \sqrt{\sum_{i=1}^{N} (\boldsymbol{B}_{ts07}^{(i)} - \boldsymbol{B}_{juno}^{(i)})^2/N} \tag{10}$$

where $\boldsymbol{B}_{ts07}^{(i)}$ are magnetic fields from Equ. 9. $\boldsymbol{B}_{juno}^{(i)}$ are the corresponding values from in-situ magnetometer data of the Juno spacecraft. N is the total number of the data. This criterion provides the best approximation to $a_{\alpha\beta}^{(\gamma)}$ and provide the best estimation of the magnetic field from the equatorial current system. In the TS07 method, the electric current flow direction is strictly parallel to Jupiter's magnetic equator. However, this premise limits the use of the TS07 method. We assume that the current sheet could be rotated by a tilt angle and an azimuthal angle, separately. So the values of the two angles are also included in the downhill simplex algorithm.

Furthermore, we consider the curvature of the current sheet. Due to the rotating tilted dipole and effects of the solar wind flow, the current sheet deviates from equatorial plane. So we adopt a nonrigid current sheet model (Khurana, 1997) by replacing z by $z - z_{cs}$, where z_{cs} is the z coordinate of the current sheet center and defines the bowl structure of Jupiter's current sheet:

$$z_{cs} = \rho \tan(\Phi_0)[\frac{x_0}{x_{jso}} \tanh(\frac{x_{jso}}{x_0}) \cos(\phi - \delta) + \cos\phi] \tag{11}$$

where Φ_0 is the tilt angle of the dipole axis from the rotation axis. x_0 and δ are parameters and their values can be found in Khurana (1997). ρ and ϕ are in Jupiter's magnetic coordinates. x_{jso} is the distance along the Jupiter-Sun axis.

In the current sheet modeling, we only use Juno's in-situ data from PJ0 to PJ20. Data beyond PJ20 are used for validation of the model. In addition, data in regions $< 5R_j$ or $> 60R_j$ are excluded. Because the influence of the currents on the magnetopause is significant beyond 60 R_j and the field within 5 R_j is dominated by the planetary field that is so strong (>1600 nT). After iterations, the best values of $a_{\alpha\beta}^{(\gamma)}$ are obtained and

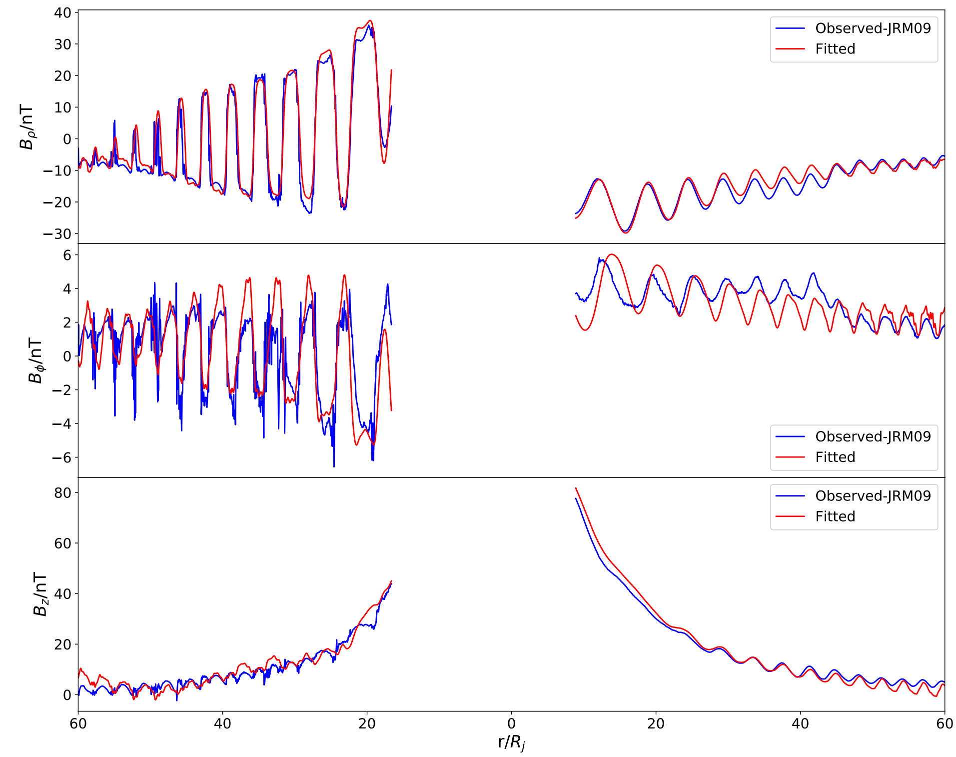

Figure 7. Observed and modeled fields from the current sheet in cylindrical components for Juno perijove 17. The observed field is the data of the magnetometer with the JRM09 internal field subtracted. The fields are plotted versus spherical radial distance with inbound data shown on the left and outbound data on the right.

are provided in the Appendix section. In addition, the best-fitting results show that the optimized current sheet is tilted by 0.85 ° from the magnetic equator and rotated by 8.81 ° in the azimuthal direction.

As an example, the fitted results of PJ17 data are shown in Fig. 7. The TS07 method based model fits the Juno data very well for B_ρ and B_z. The fluctuation of inbound B_ϕ and the sudden decrease of outbound B_ϕ near 40 R_j could not be reproduced by this model perfectly. In general, the error (σ_{cur}) of this model is 4.61 nT, which is good enough for use. Comparing with other Juno-data-based models, Pensionerov, Alexeev, et al. (2019) did not compare the results of the PCD model with B_ϕ data. In the model from Pensionerov, Belenkaya, et al. (2019), B_ϕ component was not adequately described because radial currents in magnetodisk are not included. So the inclusion of an asymmetric magnetodisc current system and radial current makes our model a more reasonable one.

Fig. 8 shows a cross-section of magnetic field lines of the current sheet model combined with the JRM09 internal model. Due to the current sheet, the field lines are stretched outward along the magnetic equator. Also shown is the color-coded azimuthal current density, which is calculated numerically from curl $\boldsymbol{B}_{cur}$. The thickness of the current sheet is assumed as $5R_j$. The current density increase with ρ if $\rho < 11R_j$ and decrease if $\rho > 11R_j$.

One advantage of the TS07 method is that the direction and symmetry of the current sheet are not assumed in advance. So a radial current system is included in our model.

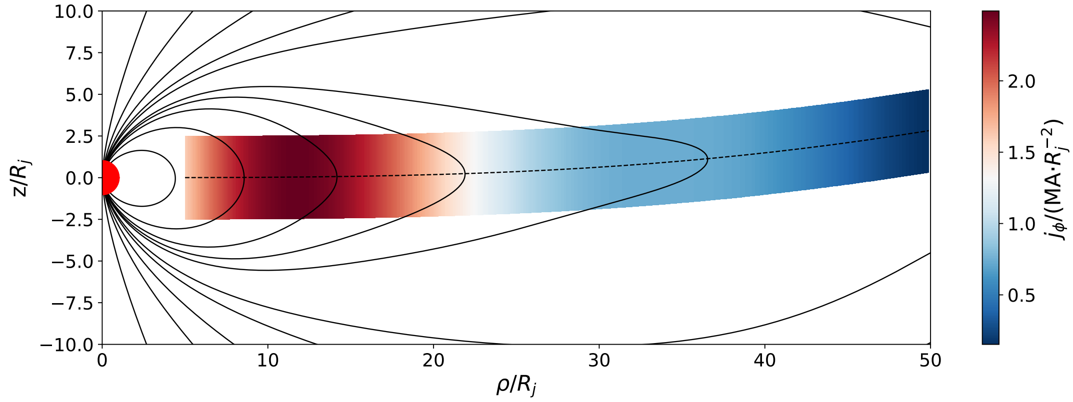

Figure 8. Cross-section of the field lines from the equatorial current system combined with the JRM09 internal field in the $\phi = 0$ meridian plane.

As a result, the sweep-back effects of the field lines are also incorporated self-consistently. This effect is a unique feature of Jupiter's magnetosphere, as shown in Fig. 9. The spiral configurations of the field lines on the dusk and dawn sectors are illustrated in the JSO coordinate system. Also shown is the magnetopause with $P_d = 0.045$ nPa.

3.5 Model validation

In this section, we will compare the results from our model with in-situ observations. To validate the applicability of our model, the data beyond PJ20 are used. These data are not used for model construction and one example of PJ21 data is shown in Fig. 10. The blue lines represent the original 1-min averaged Juno data from PDS in System III coordinates. The red lines are results from our model, including magnetic fields from the planetary dynamo, the current sheet, and the magnetopause current. The results are only shown from 5 R_j to 60 R_j for visualization reasons. Our model corresponds well with the in-situ data. So this model is suitable for magnetic field prediction in Jupiter's magnetosphere.

4 Conclusions

In this study, we attempt to develop a new global magnetic field model of Jupiter based on in-situ Juno data from PJ0 to PJ20. This modular model features a planetary dynamo, a variable magnetopause, and a cross-tail current sheet. The internal field is based on the JRM09 model, which is well determined through degree and order 10. The magnetopause shielding field is provided by minimizing the residual magnetic field component normal to the magnetopause. The variation of solar wind dynamic pressure is used to characterize the shape and currents on Jupiter's magnetopause.

In the modeling of Jupiter's current sheet, we use the TS07 method to construct an asymmetric current system, which is more reasonable comparing to the previous models. The curvature of the magnetodisk due to the solar wind effect is also incorporated in the model. As a verification, the overall error of this model for PJ17 data is 4.61 nT in the range from 5 R_j to 60 R_j. Furthermore, after minimizing the residual field component between in-situ data and the current sheet model, it is found that the magnetodisc normal is tilted from the magnetic axis by 0.85 °. The azimuthal current density peaks at $\rho \sim 11R_j$ and magnetic field lines are stretched outward along the magnetic equator. After the inclusion of the radial with currents along the current sheet, the sweep-

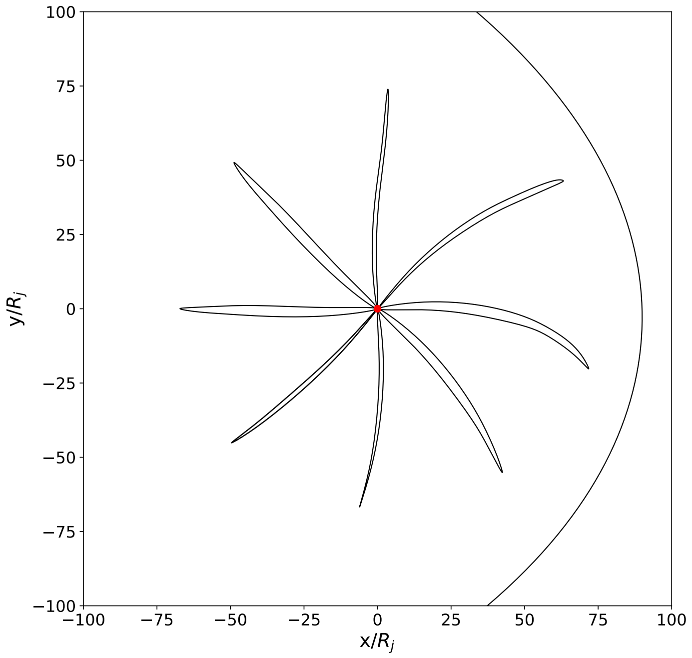

Figure 9. The view of some arbitrarily chosen field lines as seen from a point high above Jupiter.

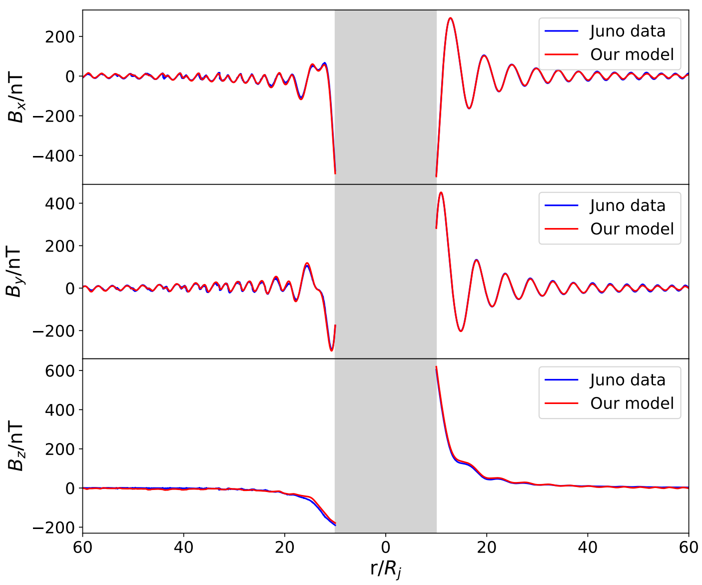

Figure 10. Comparison of the observed and the modeled vector magnetic fields for PJ21.

Table A1. Values of a^o_{mn} in Equ. 9. The row number corresponds with m-index and the column number corresponds with n-index.

(m,n)	1	2	3	4	5	6	7	8	9	10
1	1.17e2	-2.1e2	-2.4e2	4.9e2	-7.6e1	-2.6e2	-9.3e0	2.1e2	4.0e1	-1.2e2
2	-5.4e2	3.1e2	-3.2e0	-7.9e1	-3.5e1	4.9e1	5.6e1	-1.8e1	-7.7e1	3.3e1
3	5.6e2	-2.3e2	-4.0e0	5.3e1	2.7e1	-2.9e1	-4.1e1	2.1e1	6.2e1	-5.7e1
4	4.5e3	-5.1e2	-4.1e1	1.9e1	2.3e1	1.0e1	-8.4e0	-1.1e1	5.8e0	8.8e0
5	-2.8e4	1.1e3	1.4e2	1.8e1	-1.3e1	-2.3e1	-1.6e1	1.2e1	3.1e1	-3.0e1
6	6.3e4	-2.3e3	-2.6e1	3.5e1	2.0e1	7.3e0	-4.1e0	-1.2e1	-6.9e0	1.6e1
7	1.3e6	-6.8e3	-6.9e2	-1.1e2	-1.7e1	5.7e0	1.1e1	1.1e1	3.9e0	-1.5e1
8	-2.4e7	1.1e5	3.0e3	1.1e2	-2.5e1	-2.0e1	-1.1e1	-6.5e0	-2.0e0	6.3e0
9	1.8e8	-3.2e5	-9.1e3	-6.0e2	-3.5e1	1.6e1	1.6e1	1.1e1	4.5e0	-6.3e0
10	6.3e9	-6.2e6	-9.7e4	-3.7e3	-1.7e1	1.1e2	6.7e1	3.3e1	8.4e0	-1.7e1

Table A2. Values of a^e_{mn} in Equ. 9. The row number corresponds with m-index and the column number corresponds with n-index.

(m,n)	1	2	3	4	5	6	7	8	9	10
1	-3.7e2	4.0e2	-1.7e2	-1.3e2	8.4e1	9.7e1	-6.1e1	-8.2e1	7.3e1	-2.5e1
2	1.3e2	-8.1e1	2.2e1	2.8e1	5.4e0	-1.8e1	-1.8e1	3.3e0	2.7e1	-1.2e1
3	-3.6e2	1.9e2	-1.8e1	-3.4e1	-8.7e0	1.8e1	1.3e1	-1.2e1	-1.0e1	1.0e1
4	-6.9e3	7.3e2	6.4e1	-2.2e1	-2.8e1	-1.1e1	1.0e1	8.2e0	-1.2e1	6.0e0
5	2.3e4	-1.2e3	-1.2e2	-7.5e0	1.4e1	1.8e1	1.1e1	-9.8e0	-2.4e1	1.4e1
6	2.5e5	-7.3e3	-3.0e2	3.7e1	4.2e1	2.4e1	1.6e0	-2.2e1	-2.5e1	3.4e1
7	1.1e6	-2.0e4	-3.3e2	9.5e1	4.8e1	1.4e1	-4.9e0	-1.6e1	-1.2e1	2.4e1
8	7.8e6	-9.4e4	-1.1e3	1.5e2	6.4e1	1.9e1	4.0e0	-1.1e0	-1.6e0	-2.2e0
9	-4.8e8	9.8e5	2.4e4	1.2e3	1.8e0	-7.2e1	-5.3e1	-3.0e1	-7.7e0	2.4e1
10	-5.5e9	5.9e6	9.4e4	3.8e3	3.3e1	-1.2e2	-7.7e1	-3.8e1	-8.7e0	2.4e1

Table A3. Values of a^s_n in Equ. 9.

n	1	2	3	4	5	6	7	8	9	10
	5.0e2	-1.3e2	1.2e3	2.3e2	-3.3e2	5.1e2	5.8e2	-7.4e1	-4.7e2	6.9e2

back effects of Jupiter's magnetic field can also be illustrated by this model. Incorporating different parts of the modular model, we also compare the model with Juno's PJ21 data. The results show that the model can reproduce the observations well.

Acknowledgments

The authors would like to thank the Planetary Data System (PDS) of NASA for providing the data of magnetometer on the Juno spacecraft. These data can be retrieved at https://pds-ppi.igpp.ucla.edu. The authors would also like to thank J. Connerney from Goddard Space Flight Center of NASA for providing the coefficients of the JRM09 model. These coefficients can be found in the supporting information of Connerney et al. (2018).

Appendix A Fitting coefficients of TS07 method

References

Acuna, M. H., & Ness, N. F. (1976). The main magnetic field of jupiter. *Journal of Geophysical Research (1896-1977)*, *81*(16), 2917-2922. doi: 10.1029/JA081i016p02917

Alexeev, I. I., & Belenkaya, E. S. (2005). Modeling of the jovian magnetosphere. *Annales Geophysicae*, *23*(3), 809-826. doi: 10.5194/angeo-23-809-2005

Arridge, C. S., Kane, M., Sergis, N., Khurana, K. K., & Jackman, C. M. (2015). Sources of local time asymmetries in magnetodiscs. *Space Science Reviews*, *187*(1), 301-303. doi: 10.1007/s11214-015-0145-z

Bagenal, F. (1994). Empirical model of the io plasma torus: Voyager measurements. *Journal of Geophysical Research: Space Physics*, *99*(A6), 11043-11062. doi: 10.1029/93JA02908

Bagenal, F., Adriani, A., Allegrini, F., Bolton, S. J., Bonfond, B., Bunce, E. J., … Zarka, P. (2017). Magnetospheric science objectives of the juno mission. *Space Science Reviews*, *213*(1), 219-287. doi: 10.1007/s11214-014-0036-8

Bagenal, F., & Wilson, R. J. (2016). *Jupiter coordinate systems* (Tech. Rep.). University of Colorado.

Collier, M. R., Gruesbeck, J. R., Connerney, J. E. P., Joy, S. P., Hospodarsky, G. B., Roberts, A., … Roelof, E. C. (2020). A k-means clustering analysis of the jovian and terrestrial magnetopauses: A technique to classify global magnetospheric behavior. *Journal of Geophysical Research: Planets*, *125*(9), e2019JE006366. doi: 10.1029/2019JE006366

Connerney, J. E. P., Acuña, M. H., & Ness, N. F. (1981). Modeling the jovian current sheet and inner magnetosphere. *Journal of Geophysical Research: Space Physics*, *86*(A10), 8370-8384. doi: 10.1029/JA086iA10p08370

Connerney, J. E. P., Acuña, M. H., & Ness, N. F. (1982). Voyager 1 assessment of jupiter's planetary magnetic field. *Journal of Geophysical Research: Space Physics*, *87*(A5), 3623-3627. doi: 10.1029/JA087iA05p03623

Connerney, J. E. P., Acuña, M. H., Ness, N. F., & Satoh, T. (1998). New models of jupiter's magnetic field constrained by the io flux tube footprint. *Journal of Geophysical Research: Space Physics*, *103*(A6), 11929-11939. doi: 10.1029/97JA03726

Connerney, J. E. P., Benn, M., Bjarno, J. B., Denver, T., Espley, J., Jorgensen, J. L., … Smith, E. J. (2017). The juno magnetic field investigation. *Space Science Reviews*, *213*(1), 39-138. doi: 10.1007/s11214-017-0334-z

Connerney, J. E. P., Kotsiaros, S., Oliversen, R. J., Espley, J. R., Joergensen, J. L., Joergensen, P. S., … Levin, S. M. (2018). A new model of jupiter's magnetic field from juno's first nine orbits. *Geophysical Research Letters*, *45*(6), 2590-2596. doi: 10.1002/2018GL077312

Connerney, J. E. P., Timmins, S., Herceg, M., & Joergensen, J. L. (2020). A jovian magnetodisc model for the juno era. *Journal of Geophysical Research: Space Physics*, *125*(10), e2020JA028138. doi: 10.1029/2020JA028138

Cowley, S. W., Nichols, J. D., & Bunce, E. J. (2002). Distributions of current and auroral precipitation in jupiter's middle magnetosphere computed from steady-state hill-pontius angular velocity profiles: solutions for current sheet and dipole magnetic field models. *Planetary and Space Science*, *50*(7), 717-734. doi: 10.1016/S0032-0633(02)00046-6

Dougherty, M. K., Balogh, A., Southwood, D. J., & Smith, E. J. (1996). Ulysses assessment of the jovian planetary field. *Journal of Geophysical Research: Space Physics*, *101*(A11), 24929-24941. doi: 10.1029/96JA02385

Fieseler, P. D., Ardalan, S. M., & Frederickson, A. R. (2002). The radiation effects on galileo spacecraft systems at jupiter. *IEEE Transactions on Nuclear Science*, *49*(6), 2739-2758. doi: 10.1109/TNS.2002.805386

Jones, C. (2014). A dynamo model of jupiter's magnetic field. *Icarus*, *241*, 148 - 159. doi: 10.1016/j.icarus.2014.06.020

Joy, S. P., Kivelson, M. G., Walker, R. J., Khurana, K. K., Russell, C. T., & Ogino, T. (2002). Probabilistic models of the jovian magnetopause and bow shock locations. *Journal of Geophysical Research: Space Physics*, *107*(A10), SMP 17-1-SMP 17-17. doi: 10.1029/2001JA009146

Khurana, K. K. (1997). Euler potential models of jupiter's magnetospheric field. *Journal of Geophysical Research: Space Physics*, *102*(A6), 11295-11306. doi: 10.1029/97JA00563

Khurana, K. K., & Schwarzl, H. K. (2005). Global structure of jupiter's magnetospheric current sheet. *Journal of Geophysical Research: Space Physics*, *110*(A7), A07227. doi: 10.1029/2004JA010757

Lorch, C. T. S., Ray, L. C., Arridge, C. S., Khurana, K. K., Martin, C. J., & Bader, A. (2020). Local time asymmetries in jupiter's magnetodisc currents. *Journal of Geophysical Research: Space Physics*, *125*(2), e2019JA027455. doi: 10.1029/2019JA027455

McComas, D. J., Allegrini, F., Bagenal, F., Ebert, R. W., Elliott, H. A., Nicolaou, G., ... Weidner, S. (2017). Jovian deep magnetotail composition and structure. *Journal of Geophysical Research: Space Physics*, *122*(2), 1763-1777. doi: 10.1002/2016JA023039

McComas, D. J., Bagenal, F., & Ebert, R. W. (2014). Bimodal size of jupiter's magnetosphere. *Journal of Geophysical Research: Space Physics*, *119*(3), 1523-1529. doi: 10.1002/2013JA019660

Moore, K. M., Yadav, R. K., Kulowski, L., Cao, H., Bloxham, J., Connerney, J. E. P., ... Levin, S. M. (2018). A complex dynamo inferred from the hemispheric dichotomy of jupiter's magnetic field. *Nature*, *561*(7721), 76-78. doi: 10.1038/s41586-018-0468-5

Pensionerov, I. A., Alexeev, I. I., Belenkaya, E. S., Connerney, J. E. P., & Cowley, S. W. H. (2019). Model of jupiter's current sheet with a piecewise current density. *Journal of Geophysical Research: Space Physics*, *124*(3), 1843-1854. doi: 10.1029/2018JA026321

Pensionerov, I. A., Belenkaya, E. S., Cowley, S. W. H., Alexeev, I. I., Kalegaev, V. V., & Parunakian, D. A. (2019). Magnetodisc modelling in jupiter's magnetosphere using juno magnetic field data and the paraboloid magnetic field model. *Annales Geophysicae*, *37*(1), 101-109. doi: 10.5194/angeo-37-101-2019

Press, W., Flannery, B., Teukolsky, S., & W.T., V. (1992). *Numerical recipes.* Cambridge University Press.

Randall, B. A. (1998). An improved magnetic field model for jupiter's inner magnetosphere using a microsignature of amalthea. *Journal of Geophysical Research: Space Physics*, *103*(A8), 17535-17542. doi: 10.1029/98JA01437

Riddle, A. C., & Warwick, J. W. (1976). Redefinition of system iii longitude. *Icarus*, *27*(3), 457 - 459. doi: 10.1016/0019-1035(76)90025-7

Russell, C. T., Georgilas, S., Mauk, B. H., & Williams, D. J. (2004). Io as the trigger of energetic electron disturbances in the inner jovian magnetosphere. *Advances in Space Research*, *34*(11), 2242-2246. doi: 10.1016/j.asr.2003.09.065

Sitnov, M. I., Tsyganenko, N. A., Ukhorskiy, A. Y., & Brandt, P. C. (2008). Dynamical data-based modeling of the storm-time geomagnetic field with enhanced spatial resolution. *Journal of Geophysical Research: Space Physics*, *113*(A7), A07218. doi: 10.1029/2007JA013003

Stallard, T. S., Burrell, A. G., Melin, H., Fletcher, L. N., Miller, S., Moore, L., ... Johnson, R. E. (2018). Identification of jupiter's magnetic equator through h3+ ionospheric emission. *Nature Astronomy*, *2*(10), 773-777. doi: 10.1038/s41550-018-0523-z

Stephens, G. K., Sitnov, M. I., Ukhorskiy, A. Y., Roelof, E. C., Tsyganenko, N. A., & Le, G. (2016). Empirical modeling of the storm time innermost magnetosphere using van allen probes and themis data: Eastward and banana currents. *Journal of Geophysical Research: Space Physics*, *121*(1), 157-170. doi: 10.1002/2015JA021700

Tao, C., Kataoka, R., Fukunishi, H., Takahashi, Y., & Yokoyama, T. (2005). Magnetic field variations in the jovian magnetotail induced by solar wind dynamic pressure enhancements. *Journal of Geophysical Research: Space Physics*, *110*(A11), A11208. doi: 10.1029/2004JA010959

Tsyganenko, N. A. (1995). Modeling the earth's magnetospheric magnetic field confined within a realistic magnetopause. *Journal of Geophysical Research: Space Physics*, *100*(A4), 5599-5612. doi: 10.1029/94JA03193

Tsyganenko, N. A. (2013). Data-based modelling of the earth's dynamic magnetosphere: a review. *Annales Geophysicae*, *31*(10), 1745–1772. doi: 10.5194/angeo-31-1745-2013

Tsyganenko, N. A., & Sitnov, M. I. (2007). Magnetospheric configurations from a high-resolution data-based magnetic field model. *Journal of Geophysical Research: Space Physics*, *112*(A6), A06225. doi: 10.1029/2007JA012260

Wang, J., Ma, J., Qiu, J., Tian, D., Zhu, A., Zhang, Q., & Zhou, A. (2019). Optimization design of radiation vault in jupiter orbiting mission. *IEEE Transactions on Nuclear Science*, *66*(10), 2179-2187. doi: 10.1109/TNS.2019.2939184

Wang, J., Zhang, Q., Zheng, Y., Tian, D., Zhu, A., Qiu, J., & Ma, J. (2019). Tid and internal charging evaluation for jupiter orbiting mission. *IEEE Transactions on Nuclear Science*, *66*(2), 557-566. doi: 10.1109/TNS.2018.2890660

Zieger, B., & Hansen, K. C. (2008). Statistical validation of a solar wind propagation model from 1 to 10 au. *Journal of Geophysical Research: Space Physics*, *113*(A8), A08107. doi: 10.1029/2008JA013046